PNAS RESEARCH ARTICLE | IMMUNOLOGY AND INFLAMMATION OPEN ACCESS

Asymmetric arginine dimethylation of cytosolic RNA and DNA sensors by PRMT3 attenuates antiviral innate immunity

Junji Zhu[a,b,1], Xiong Li[a,b,1], Xiaolian Cai[a,c], Ziwen Zhou[a,b], Qian Liao[a,b], Xing Liu[a,b,c], Jing Wang[a,b,c], and Wuhan Xiao[a,b,c,d,2]

Edited by Pinghui Feng, University of Southern California, Los Angeles, CA; received September 1, 2022; accepted July 19, 2023 by Editorial Board Member Adolfo Garcia-Sastre

The cytosolic RNA and DNA sensors initiate type I interferon signaling when binding to RNA or DNA. To effectively protect the host against virus infection and concomitantly avoid excessive interferonopathy at resting states, these sensors must be tightly regulated. However, the key molecular mechanisms regulating these sensors' activation remain elusive. Here, we identify PRMT3, a type I protein arginine methyltransferase, as a negative regulator of cytosolic RNA and DNA sensors. PRMT3 interacts with RIG-I, MDA5, and cGAS and catalyzes asymmetric dimethylation of R730 on RIG-I, R822 on MDA5, and R111 on cGAS. These modifications reduce RNA-binding ability of RIG-I and MDA5 as well as DNA-binding ability and oligomerization of cGAS, leading to the inhibition of downstream type I interferon production. Furthermore, mice with loss of one copy of *Prmt3* or in vivo treatment of the PRMT3 inhibitor, SGC707, are more resistant to RNA and DNA virus infection. Our findings reveal an essential role of *PRMT3* in the regulation of antiviral innate immunity and give insights into the molecular regulation of cytosolic RNA and DNA sensors' activation.

PRMT3 | RIG-I | MDA5 | cGAS | innate immunity

Significance

As the first line of defense against virus infection, innate immunity must be tightly controlled. Type I interferon signaling is initiated when the cytosolic RNA sensors, RIG-I and MDA5, bind to viral RNAs and the cytosolic DNA sensor, cGAS, binds to viral DNAs. However, how these sensors are regulated at the resting state and during viral infection remains largely unknown. In this study, we identified that PRMT3 catalyzes asymmetric arginine dimethylation of RIG-I, MDA5, and cGAS, leading to the inhibition of their activation. As a result, knockdown of Prmt3 in mice can protect mice against both RNA and DNA virus infection. Our results suggest that PRMT3 is a negative regulator of cytosolic RNA and DNA sensors.

In the nature, organisms are continuously assaulted by invading pathogens. Innate immunity is a powerful host-defense system against pathogen invasions. Activation of innate immunity requires the recognition of pathogen-associated molecular patterns (PAMPs) through pattern-recognition receptors (PRRs) (1). As the members of PAMPs, pathogen-derived nucleic acids are crucial signals for innate immunity (2). Within the cytosol of mammalian cells, the detection of pathogen-derived nucleic acids is mainly carried out by two sensing systems: the RLR-MAVS pathway for the recognition of RNA species and the cGAS–STING pathway for the recognition of DNA (1–6). Activation of these two pathways triggers diverse types of downstream effect responses that eventually lead to the production of type I interferon (IFN) and proinflammatory cytokines (7). Although to efficiently activate innate immunity is essential for the host to restrict viral infection, aberrant and excessive activation of innate immunity results in the pathogenesis of autoimmune diseases. Therefore, tight control of innate immunity is critical for protecting host against viral infection as well as avoiding harmful immunopathology (1).

During RNA virus infection, cytosolic viral RNAs are recognized by retinoic acid–inducible–like receptors (RLRs), including retinoic acid–inducible gene 1 protein (RIG-I) and melanoma differentiation–associated gene 5 (MDA5) (8, 9). RIG-I primarily recognizes single-strand or double-strand RNA with a 5′-triphosphorylated (PPP) group (9–12), whereas MDA5 primarily recognizes long viral dsRNAs or dsRNA replication intermediates (8, 9, 13). Recognition of viral RNAs by RLRs leads to the activation of the adaptor protein MAVS (also known as VISA, IPS-1, and Cardif) (14–18). During DNA virus infection, dsDNA or the DNA-RNA hybrids derived from DNA viruses are sensed and catalyzed by the cyclic GMP-AMP (cGAMP) synthase (cGAS) to synthesize the second messenger molecule cGAMP, which induces the oligomerization of the adaptor protein STING (also known as MITA and ERIS), thereby activating STING. Activation of MAVS and STING results in stimulation of the kinase TBK1 and IKK, leading to activating the transcription factors IRF3, IRF7, and nuclear factor kB (NF-KB) (2).

Protein arginine methylation catalyzed by protein arginine methyltransferases (PRMTs) is an abundant posttranslational modification (PTM) in histone and nonhistone proteins of eukaryotes that can affect numerous cellular activities, including transcription and chromatin regulation, cell signaling, DNA damage response, RNA expression, and cellular metabolism (19–21). PRMTs are composed of nine members (*PRMT1-9*), which are classified into three categories depending on the modification they catalyze (19). Type I (PRMT1, PRMT2, PRMT3, PRMT4, PRMT6, and PRMT8) and type II (PRMT5 and PRMT9) enzymes catalyze the formation of monomethylarginine (MMA) as an intermediate before the establishment of asymmetric dimethylarginine (aDMA) or symmetric

Author affiliations: [a]State Key Laboratory of Freshwater Ecology and Biotechnology, Institute of Hydrobiology, Chinese Academy of Sciences, Wuhan 430072, People's Republic of China; [b]Hubei Hongshan Laboratory, Wuhan 430070, People's Republic of China; [c]University of Chinese Academy of Sciences, Beijing 100049, People's Republic of China; and [d]The Innovation of Seed Design, Chinese Academy of Sciences, Wuhan 430072, People's Republic of China

Author contributions: J.Z., X. Li, and W.X. designed research; J.Z. and X. Li performed research; X.C., Z.Z., Q.L., X. Liu, and J.W. contributed new reagents/analytic tools; J.Z., X. Li, and W.X. analyzed data; and J.Z., X. Li, and W.X. wrote the paper.

The authors declare no competing interest.

This article is a PNAS Direct Submission. P.F. is a guest editor invited by the Editorial Board.

[1]J.Z. and X.L. contributed equally to this work.

[2]To whom correspondence may be addressed. Email: w-xiao@ihb.ac.cn.

This article contains supporting information online at https://www.pnas.org/lookup/suppl/doi:10.1073/pnas.2214956120/-/DCSupplemental.

Published August 28, 2023.

dimethylarginine (sDMA), respectively (19). PRMT7 is a type III enzyme that catalyzes the formation of MMA (22). Accumulating evidence support an essential role of PRMTs in the antiviral immune response (23–31). As reported, PRMT6 attenuates the antiviral immune response by blocking TBK1-IRF3 signaling (23). PRMT1 promotes the antiviral immune response by catalyzing asymmetric arginine methylation of TBK1 (28). PRMT5 attenuates cGAS-mediated antiviral immune response either by catalyzing methylation of IFI16 (or its murine homolog IFI204) or by directly catalyzing symmetric dimethylation of cGAS at the Arg^{124} (29, 30). Nuclear cGAS recruits Prmt5 and facilitates Prmt5-mediated H3R2me2s modification at the promoters of type I IFNs, leading to the enhancement of antiviral immunity in response to RNA and DNA virus infections (31). Symmetric arginine dimethylation of the spliceosome is required for the production of type I and III interferons (32). PRMT7 negatively regulates the RLR signaling by catalyzing MAVS monomethylation at Arg^{52} (25, 27).

As a type I arginine methyltransferase, PRMT3 is essential for the proper maturation of the 80S ribosome by binding to and catalyzing the methylation of the 40S ribosomal protein S2 (rpS2) (33). By interaction with rpS2, PRMT3 plays a pivotal role in neuronal translation, contributing to activity-dependent changes in the dendritic spines (34). In addition, PRMT3 promotes tumorigenesis by targeting different molecules (35–37). Using a zebrafish model, we found that *prmt3* negatively regulates antiviral innate immunity in response to RNA virus infection (26). However, the underlying mechanism is still elusive.

Here, we further identified that *PRMT3* negatively regulates both RNA and DNA virus–triggered innate antiviral response in mammals. Mechanistic studies indicate that PRMT3 catalyzes asymmetric dimethylation of R730 on RIG-I, R822 on MDA5, and R111 on cGAS. PRMT3-mediated methylation attenuates the RNA-binding ability of RIG-I and MDA5, as well as the DNA-binding ability and oligomerization of cGAS, leading to the attenuation of type I IFN signaling.

Results

***PRMT3* Attenuates RNA and DNA Virus–Triggered Antiviral Innate Immune Response.** Our previous observation that zebrafish *prmt3* negatively regulates innate antiviral response provoked us to further investigate the underlying mechanisms of *PRMT3* in antiviral innate immunity using a mammalian system (26). Upon Sendai virus (SeV) or vesicular stomatitis virus (VSV) infection in THP-1 cells, overexpression of *PRMT3* in THP-1 cells significantly decreased the expression of *IFNB1*, *ISG56*, and *CXCL10* mRNA compared with the transfection of empty vector control (Vec.) (Fig. 1*A* and *SI Appendix*, Fig. S1*A*). In contrast, knockout of *PRMT3* in THP-1 cells (*PRMT3*-KO#1 and *PRMT3*-KO-#2) (*SI Appendix*, Fig. S1*B*) dramatically increased the expression of *IFNB1*, *ISG56*, and *CXCL10* mRNA after infection with SeV or VSV (Fig. 1 *B* and *C*). Similarly, we observed that the expression of *Ifnb, Isg56*, and *Cxcl10* was higher in *Prmt3*-dicicient mouse lung fibroblast cells (MLFs) and mouse embryonic fibroblast cells (MEFs) ($Prmt3^{-/-}$) than in the wild-type *Prmt3* MLFs and MEFs ($Prmt3^{+/+}$) after transfection with poly(I:C), or infection with SeV, VSV, or encephalomyocarditis virus (EMCV) (Fig. 1 *D–F* and *SI Appendix*, Fig. S1 *C–F*). Consistently, phosphorylation of IRF3 (p-IRF3), IκBα (p-IκBα), and STAT1 (p-STAT1) was enhanced in *PRMT3*-deficient THP-1 cells compared with that in the control cells (Fig. 1*G*). In agreement, VSV replication was inhibited in PRMT3-deficient THP-1 cells compared with that in the control cells as revealed by VSV titer determination (Fig. 1*H*). As expected, upon SeV infection, p-Irf3, p-IκBα, and p-Stat1 were enhanced in $Prmt3^{-/-}$ MLFs and MEFs compared with those in $Prmt3^{+/+}$ MLFs and MEFs (Fig. 1*I* and *SI Appendix*, Fig. S1*G*). VSV-GFP propagation was also reduced in $Prmt3^{-/-}$ MLFs compared with that in $Prmt3^{+/+}$ MLFs as revealed by the flow cytometry assay and fluorescent microscopy images (Fig. 1*J*). These data suggest that *PRMT3* negatively regulates RNA virus–triggered antiviral innate immunity.

Subsequently, we examined whether *PRMT3* has impacts on DNA virus–triggered innate antiviral response. In response to herpes simplex virus 1 (HSV-1) infection in human foreskin fibroblasts (HFF) cells, overexpression of *PRMT3* significantly decreased the expression of *IFNB1*, *ISG56*, and *CXCL10* mRNA compared with the transfection of the empty vector control (Vec.) (Fig. 2*A*). On the contrary, knockout of *PRMT3* in THP-1 cells dramatically increased the expression of *IFNB1*, *ISG56*, and *CXCL10* mRNA compared with the control cells after infection with HSV-1 (Fig. 2*B*). After stimulation with dsDNAs, HSV120 (a synthetic 120-bp dsDNA representing the genome of HSV-1), VAVC70 (a potent dsDNA immunostimulant) (38) or ISD45 (45-mer IFN-stimulatory DNA) (39–41), the expression of *IFNB1*, *ISG56*, and *CXCL10* mRNA was higher in *PRMT3*-deficient THP-1 cells than in the control cells (Fig. 2*C*). Similarly, after infection with HSV-1, MCMV (Mouse cytomegalovirus) or ECTV (Ectromelia virus), as well as stimulation with dsDNAs, HSV120, DNA90 (dsDNA of ~90 bp), or VAVC70 (41), the expression of *Ifnb, Isg56*, and *Cxcl10* mRNA was higher in $Prmt3^{-/-}$ MLFs and MEFs than in $Prmt3^{+/+}$ MLFs and MEFs (Fig. 2 *D–F* and *SI Appendix*, Fig. S1 *H–J*). Consistently, p-IRF3, p-IκBα, and p-STAT1 were enhanced in *PRMT3*-deficient THP-1 cells compared with those in the control cells (Fig. 2*G*). In agreement, HSV-1 propagation was decreased in *PRMT3*-deficient THP-1 cells compared with that in the control cells as revealed by HSV-1 titer determination (Fig.2*H*). In response to HSV-1 infection, p-Irf3, p-IκBα, and p-Stat1 were promoted in $Prmt3^{-/-}$ MLFs and MEFs compared with those in $Prmt3^{+/+}$ MLFs and MEFs (Fig. 2*I* and *SI Appendix*, Fig. S1*K*). As expected, HSV-GFP propagation was decreased in $Prmt3^{-/-}$ MLFs compared with that in $Prmt3^{+/+}$ MLFs as revealed by flow cytometry assay and fluorescent microscopy images (Fig. 2*J*).

Collectively, these data suggest that *PRMT3* attenuates RNA and DNA virus–triggered antiviral innate immunity.

Loss of One Copy of *Prmt3* and PRMT3 Inhibitor (SGC707) Treatment Promotes Antiviral Innate Immunity In Vivo. To further confirm the function of *Prmt3* in type I IFN signaling, we generated *Prmt3*-deficient mice by CRISPR-Cas9 (*SI Appendix*, Fig. S2*A*). Similar to what was reported previously, after $Prmt3^{+/-}$ mice were intercrossed, $Prmt3^{-/-}$ mice were born lower than the expected mendelian ratio with a relatively small body size (42). In addition, adult $Prmt3^{-/-}$ mice also exhibited serious deficiency in reproduction either self-intercrossing or intercrossing with $Prmt3^{+/-}$ mice. Thus, we were unable to obtain enough $Prmt3^{-/-}$ mice for subsequent viral infection experiments in this study; then, we turned to utilize $Prmt3^{+/-}$ mice for further assays (27). The expression level of *Prmt3* mRNA was substantially reduced in the spleen and lung of $Prmt3^{+/-}$ mice compared with that in $Prmt3^{+/+}$ mice (*SI Appendix*, Fig. S2*B*). Moreover, the Prmt3 protein level in the livers and spleens of $Prmt3^{+/-}$ mice was also significantly reduced compared with that in the livers and spleens of $Prmt3^{+/+}$ mice (*SI Appendix*, Fig. S2 *C* and *D*).

To evaluate the importance of *Prmt3* in the host against RNA virus infection, we intraperitoneally injected 6- to 8-wk-old $Prmt3^{+/+}$ and $Prmt3^{+/-}$ mice with EMCV and monitored their survival. The results indicated that $Prmt3^{+/-}$ mice were more resistant to

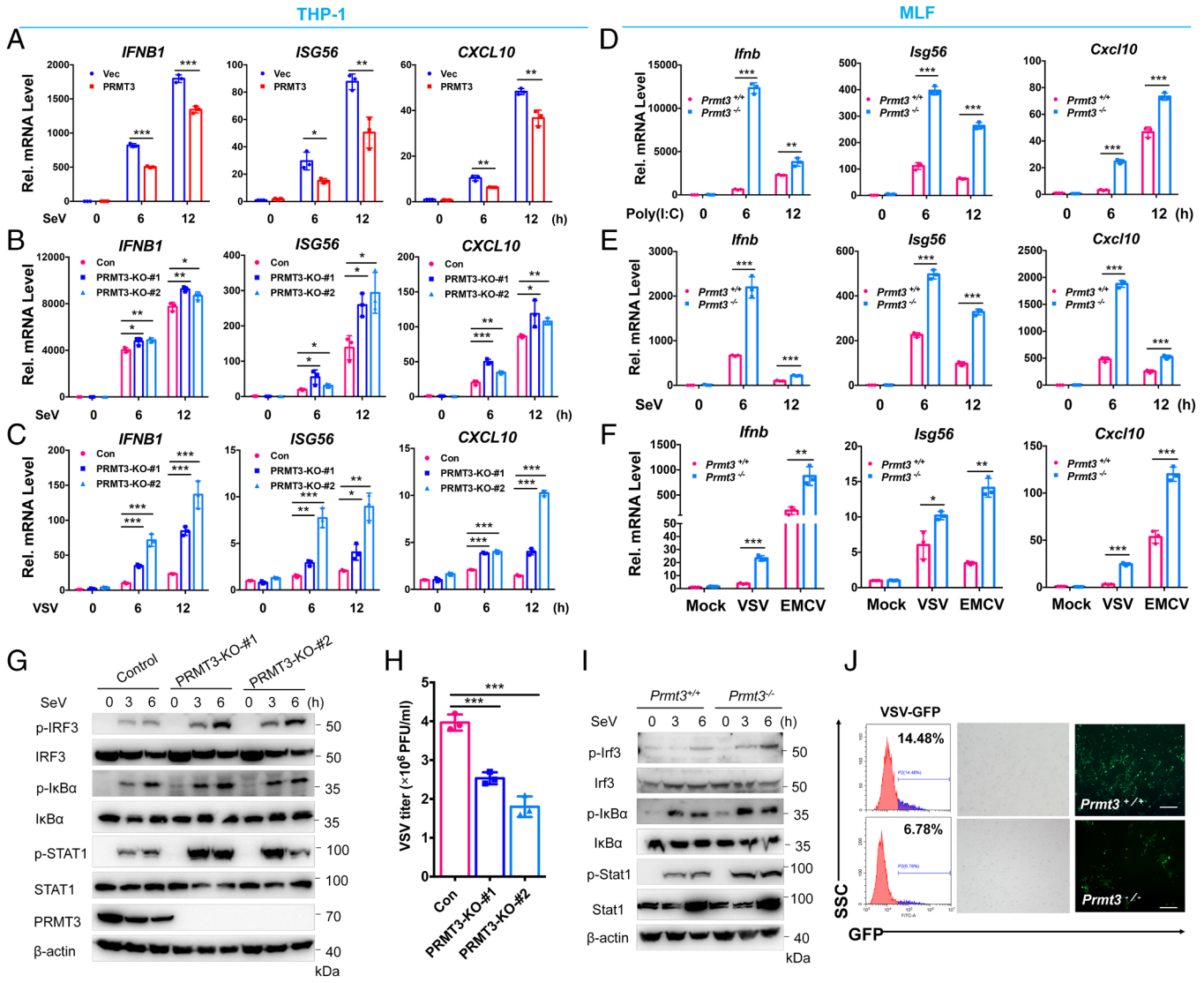

Fig. 1. *PRMT3* attenuates RNA virus–triggered antiviral innate immune response. (*A*) qRT-PCR analysis of *IFNB1, ISG56, and CXCL10* mRNA in THP-1 cells stably expressing empty vector (Vec) or PRMT3 with SeV infection for 0 to 12 h. (*B* and *C*) Effects of PRMT3 deficiency on transcription of downstream genes induced by SeV (*B*) or VSV (*C*). PRMT3-deficient (KO) THP-1 cell lines were generated by the CRISPR-Cas9 method. PRMT3-KO and control (Con) THP-1 cells were left uninfected or infected with SeV or VSV for the indicated times before qRT-PCR analysis. (*D* and *E*) qRT-PCR analysis of *Ifnb1, Isg56, and Cxcl10* mRNA in *Prmt3*$^{+/+}$ and *Prmt3*$^{-/-}$ MLF cells, followed by poly(I:C) transfection (*D*) or SeV infection (*E*) for the indicated times. (*F*) qRT-PCR analysis of *Ifnb1, Isg56, and Cxcl10* mRNA in *Prmt3*$^{+/+}$ and *Prmt3*$^{-/-}$ MLF cells with VSV or EMCV infection for 8 h. (*G*) Effects of PRMT3 deficiency on SeV-induced phosphorylation of IRF3, IκBα, and STAT1. PRMT3-KO (PRMT3-KO#1 and PRMT3-KO#2) and the control THP-1 cells (Con) were infected with SeV for the indicated times before immunoblotting analysis. (*H*) Plaque assay of VSV titers in PRMT3-KO (PRMT3-KO#1 and PRMT3-KO#2) and control (Con) THP-1 cells infected with VSV (1 MOI). (*I*) IB analysis of SeV-induced phosphorylation of Irf3, IκBα, and Stat1 in *Prmt3*$^{+/+}$ and *Prmt3*$^{-/-}$ MLFs, followed by SeV infection for the indicated times. (*J*) Flow cytometry analysis (left graphs) and microscopy imaging (right images) of the replication of VSV-GFP in *Prmt3*$^{+/+}$ and *Prmt3*$^{-/-}$ MLFs challenged with VSV-GFP (1 MOI) for 12 h; the numbers adjacent to the outlined areas indicate percentages of GFP-positive (GFP $^{+}$) MLFs. (Scale bar, 200 μm.) *P < 0.05, **P < 0.01, and ***P < 0.001, using unpaired Student's t test (*H*) or two-way ANOVA with Holm–Sidak's multiple comparisons test (*A*–*F*). Data are representative of three independent experiments (*A*–*F* and *H*; mean ± SD of three technical replicates) or represent three independent experiments (*G*, *I*, and *J*).

EMCV-induced death than the *Prmt3*$^{+/+}$ controls (Fig. 3*A*). Consistently, the IFN-β level in sera from *Prmt3*$^{+/-}$ mice infected with EMCV for 24 h was higher than that from *Prmt3*$^{+/+}$ mice (Fig. 3*B*). In agreement, the mRNA level of *Ifnb1* in the liver, spleen, and lung of *Prmt3*$^{+/-}$ mice was higher than those of *Prmt3*$^{+/+}$ mice after EMCV infection for 24 h (Fig. 3*C*). By contrast, the viral titer of EMCV in the liver, spleen, and lung of *Prmt3*$^{+/-}$ mice was lower than those of *Prmt3*$^{+/+}$ mice (Fig. 3*D*). Hematoxylin and eosin (H & E) staining of lung tissues indicated greater infiltration of immune cells and injury in the lungs of *Prmt3*$^{+/+}$ mice compared with those of *Prmt3*$^{+/-}$ mice, after infection with EMCV infection (Fig. 3*E*). Moreover, by the treatment with the PRMT3 inhibitor, SGC707, on mice (43), the IFN-β level in sera was promoted significantly, but EMCV titer in the liver, spleen, and lung was decreased dramatically (Fig. 3 *F* and *G*).

Subsequently, we examined the function of *Prmt3* in the host against DNA virus infection. After intraperitoneally injected mice with HSV-1, *Prmt3*$^{+/-}$ mice were more resistant to HSV-1-induced mortality than *Prmt3*$^{+/+}$ mice. Additionally, we observed a higher IFN-β level in sera of *Prmt3*$^{+/-}$ mice compared with *Prmt3*$^{+/+}$ mice (Fig. 3 *H* and *I*). As expected, the mRNA level of *Ifnb1* was higher in the liver, spleen, and lung of *Prmt3*$^{+/-}$ mice than those of *Prmt3*$^{+/+}$ mice after viral infection for 24 h (Fig. 3*J*). By contrast, the viral titer of HSV-1 was lower in the liver, spleen, and lung of *Prmt3*$^{+/-}$ mice than those of *Prmt3*$^{+/+}$ mice after viral infection for 24 h (Fig. 3*K*). Compared with *Prmt3*$^{+/-}$ mice, greater infiltration

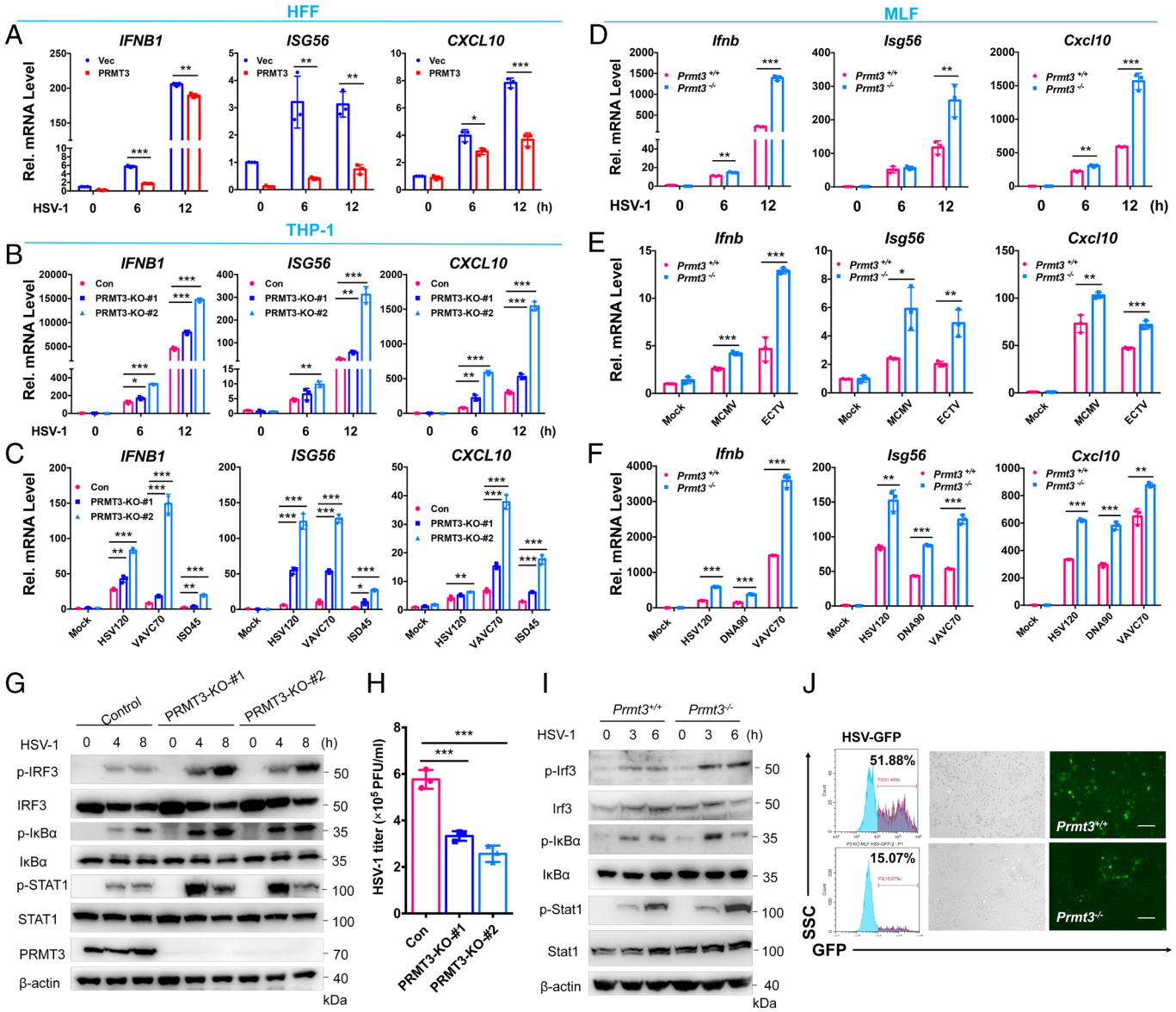

Fig. 2. *PRMT3* attenuates DNA virus–triggered antiviral innate immune response. (*A*) qRT-PCR analysis of *IFNB1, ISG56, and CXCL10* mRNA in HFF cells stably expressing empty vector (Vec) or PRMT3 with HSV-1 infection for 0 to 12 h. (*B* and *C*) Effects of PRMT3-deficiency on transcription of downstream genes induced by HSV-1 (*B*) or cytosolic dsDNA (*C*). PRMT3-KO and control (Con) THP-1 cells were left uninfected or infected with HSV-1 for the indicated times or transfected with nucleic acids (3 μg/mL) for 4 h before qRT-PCR analysis. (*D–F*) qRT-PCR analysis of *Ifnb, Isg56, Cxcl10* mRNA in $Prmt3^{+/+}$ and $Prmt3^{-/-}$ MLFs infected with HSV-1 for the indicated times (*D*) or infected with MCMV or ECTV for 8 h. (*E*) or transfected with nucleic acids (3 μg/mL) for 4 h (*F*). (*G*) Effects of PRMT3-deficiency on HSV-1-induced phosphorylation of IRF3, STAT1, and IκBα. PRMT3-KO and control THP-1 cells (Control) were left uninfected or infected with HSV-1 for the indicated times before immunoblotting analysis. (*H*) Plaque assay of HSV-1 titers in PRMT3-KO (PRMT3-KO#1 and PRMT3-KO#2) and control (Con) THP-1 cells infected with HSV-1 (1 MOI). (*I*) Immunoblotting (IB) analysis of HSV-1-induced phosphorylation of Irf3, IκBα, and Stat1 in $Prmt3^{+/+}$ and $Prmt3^{-/-}$ MLFs, followed by HSV-1 infection for the indicated times. (*J*) Flow cytometry analysis (left graphs) and microscopy imaging (right images) of the replication of HSV-GFP in $Prmt3^{+/+}$ and $Prmt3^{-/-}$ MLFs challenged with HSV-GFP (1 MOI) for 12 h, the numbers adjacent to the outlined areas indicate percentages of GFP-positive (GFP^+) MLFs. (Scale bar, 100 μm.) $^*P < 0.05$, $^{**}P < 0.01$, and $^{***}P < 0.001$, using unpaired Student's *t* test (*H*) or two-way ANOVA with Holm–Sidak's multiple comparisons test (*A–F*). Data are representative of three independent experiments (*A–F* and *H*; mean ± SD of three technical replicates), or represent two independent experiments (*G, I,* and *J*).

of immune cells and injury were observed in the lungs of $Prmt3^{+/+}$ mice (Fig. 3*L*). Treatment with SGC707 caused an increase of the IFN-β level in sera and a reduction of the HSV-1 titer in the liver, spleen, and lung of mice (Fig. 3 *M* and *N*).

To further validate the function of *Prmt3* in type I IFN signaling, we utilized mouse bone marrow–derived dendritic cells (BMDCs) isolated from $Prmt3^{+/+}$ and $Prmt3^{+/-}$ mice. After transfection with 5′-ppp-dsRNA or poly (I:C) or infection with RNA viruses, SeV, VSV, or EMCV, the expression of *Ifnb1, Isg56, Cxcl10*, and *Il6* mRNA was higher in $Prmt3^{+/-}$ BMDCs than in $Prmt3^{+/+}$ BMDCs (*SI Appendix*, Fig. S2*E*). In agreement, p-Tbk1 and p-Irf3 were enhanced in $Prmt3^{+/-}$ BMDC cells compared with in $Prmt3^{+/+}$ BMDCs upon SeV infection (*SI Appendix*, Fig. S2*F*). Similar results were obtained in the case of stimulation with viral DNA mimics, ISD45 and VACV70, and infections with DNA viruses, HSV-1 and ECTV (*SI Appendix*, Fig. S2 *G* and *H*). Consistently, viral propagation indicated by VSV-N, EMCV-3D, and HSV-1-genome copies was dramatically attenuated in $Prmt3^{+/-}$ BMDCs compared with in $Prmt3^{+/+}$ BMDCs after infection with VSV, EMCV, or HSV-1 for 8 h (*SI Appendix*, Fig. S2*I*).

Taken together, these data suggest that loss of one copy of *Prmt3* and its enzymatic activity inhibition protect the host against RNA and DNA virus infection in vivo.

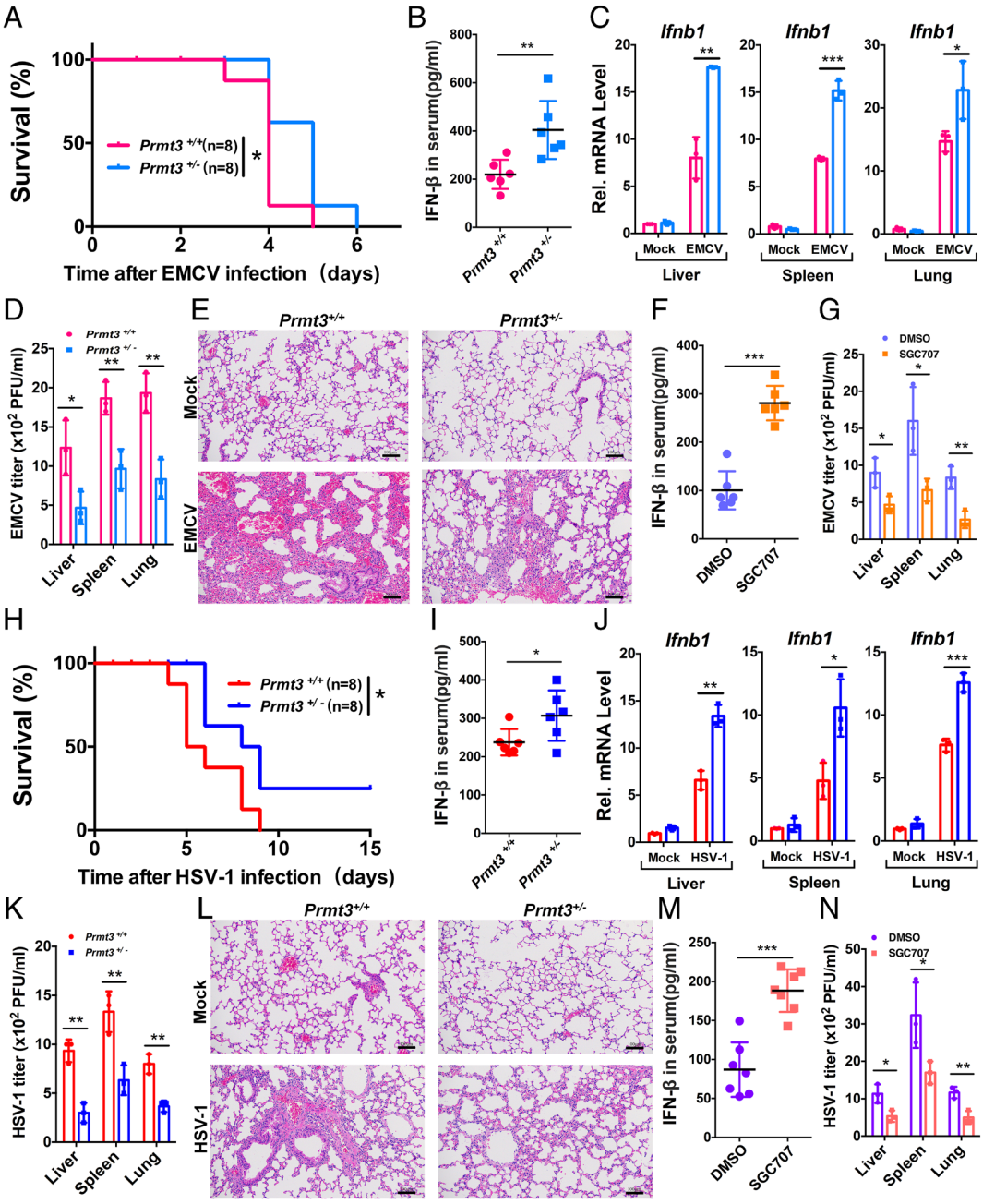

Fig. 3. Loss of one copy of *Prmt3* and treatment with PRMT3 inhibitor SGC707 protect mice from RNA and DNA virus infection. (*A*) Survival (Kaplan–Meier curve) of *Prmt3*$^{+/+}$ and *Prmt3*$^{+/-}$ mice (8 mice/per group) at the indicated times after intraperitoneal infection with EMCV (1 × 10^6 PFU/per mouse). (*B*) ELISA of IFN-β in the serum from *Prmt3*$^{+/+}$ and *Prmt3*$^{+/-}$ mice (6 mice/per group) given intraperitoneal injection of EMCV (1 × 10^6 PFU/per mouse) for 24 h. (*C*) qRT-PCR analysis of *Ifnb* mRNA in the liver (*Left*), spleen (*Middle*), and lung (*Right*) of *Prmt3*$^{+/+}$ and *Prmt3*$^{+/-}$ mice (3 mice/per group) given intraperitoneal injection of EMCV (1 × 10^6 PFU/per mouse) for 24 h. (*D*) Plaque assay of EMCV titers in the livers, spleens, and lungs of infected mice as in *C*. (*E*) Microscopy of H.& E.-stained lung sections from mice treated with PBS or EMCV as in *C*. (Scale bar, 100 μm.) (*F*) ELISA of IFN-β in the serum from WT mice (6 mice/per group) pretreated with SGC707 (30 mg/kg, i.p.) and given intraperitoneal injection of EMCV (1 × 10^6 PFU/per mouse) for 24 h. (*G*) Plaque assay of EMCV titers in the livers, spleens, and lungs from WT mice (3 mice/per group) pretreated with SGC707 (30 mg/kg, i.p.) and given intraperitoneal injection of EMCV (1 × 10^6 PFU/per mouse) for 24 h. (*H*) Survival (Kaplan–Meier curve) of *Prmt3*$^{+/+}$ and *Prmt3*$^{+/-}$ mice (8 mice/per group) at various times after intraperitoneal infection with EMCV (1 × 10^6 PFU/per mouse). (*I*) ELISA of IFN-β in the serum from *Prmt3*$^{+/+}$ and *Prmt3*$^{+/-}$ mice (6 mice/per group) given intraperitoneal injection of HSV-1 (1 × 10^6 PFU/per mouse) for 24 h. (*J*) qRT-PCR analysis of *Ifnb* mRNA in the livers (*Left*), spleens (*Middle*), and lungs (*Right*) of *Prmt3*$^{+/+}$ and *Prmt3*$^{+/-}$ mice (3 mice/per group) given intraperitoneal injection of HSV-1 (1 × 10^7 PFU/per mouse) for 24 h. (*K*) Plaque assay of HSV-1 titers in the livers, spleens, and lungs of infected mice as in *J*. (*L*) Microscopy of H & E-stained lung sections from mice treated with PBS or HSV-1 as in *J*. (Scale bar, 100 μm.) (*M*) ELISA of IFN-β in the serum from WT mice (7 mice/per group) pretreated with SGC707 (30 mg/kg, i.p.) and given intraperitoneal injection of HSV-1 (1 × 10^7 PFU/per mouse) for 24 h. (*N*) Plaque assay of HSV-1 titers in the livers, spleens, and lungs from WT mice (3 mice/per group) pretreated with SGC707 (30 mg/kg, i.p.) and given intraperitoneal injection of HSV-1 (1 × 10^7 PFU/per mouse) for 24 h. *P < 0.05, **P < 0.01, and ***P < 0.001, using unpaired Student's t test (*B, F, I,* and *M*) or two-way ANOVA with Holm–Sidak's multiple comparisons test (*C, D, G, J, K,* and *N*) or the log-rank (Mantel-Cox) test (*A* and *H*). Data are representative of three independent experiments (*C, D, G, J, K* and *N*; mean ± SD of three biological replicates) or represent two independent experiments (*A, B, E, F, H, I, L,* and *M*; mean ± SD in *B, F, I,* and *M*).

PRMT3 Attenuates Innate Antiviral Response via Its Methyltransferase Activity. Given that PRMT3 belongs to one of the type I arginine methyltransferases, we aimed to determine whether the inhibitory effect of PRMT3 on type I IFN signaling relies on PRMT3's enzymatic activity. Initially, we compared the impact of wild-type PRMT3 with its enzymatically inactive mutant,

PRMT3-3M (G263A/C264A/G265A) (44). In *Prmt3*$^{-/-}$ MLFs, overexpression of wild-type PRMT3 significantly suppressed the expression of *Ifnb*, *Isg56*, and *Cxcl10* mRNA upon SeV or HSV-1 infection, whereas PRMT3-3M had no such effect (Fig. 4 *A* and *B*). Consistently, the phosphorylation of Tbk1 and Irf3 was attenuated by wild-type PRMT3 but not by PRMT3-3M in response to SeV or HSV-1 infection (Fig. 4 *C* and *D*).

Furthermore, in *PRMT3*-deficient H1299 cells (*PRMT3*$^{-/-}$) (Fig. 4*E*), overexpression of PRMT3 markedly promoted VSV-GFP and HSV-GFP propagation, but overexpression of PRMT3-3M did not exhibit the same effect (Fig. 4 *F* and *G*).

In MLFs, treatment with SGC707 enhanced the expression of *Ifnb, Isg56*, and *Cxcl10* mRNA significantly in response to SeV or HSV-1 infection (Fig. 4 *H* and *I*). In agreement, treatment with SGC707 also promoted p-TBK1 and p-IRF3 (Fig. 4 *J* and *K*), while suppressing the propagation of VSV-GFP and HSV-GFP (Fig. 4*L*).

Collectively, these data suggest that the suppressive role of *PRMT3* on antiviral innate immunity is dependent on its enzymatic activity.

PRMT3 Targets Cytosolic RNA Sensors RIG-I and MDA5 as well as DNA Sensor cGAS, to Catalyze Their Arginine Dimethylation. To determine the underlying mechanisms of *PRMT3* in innate immunity in response to RNA and DNA virus infection, we examined the interaction between PRMT3 and the molecules in both the RIG-I-MAVS pathway and the cGAS–STING pathway by coimmunoprecipitation assays. As shown in Fig. 5*A*, overexpressed PRMT3 interacted with cGAS, RIG-I, and MDA5. We further confirmed these interactions by conducting coimmunoprecipitation assays (*SI Appendix*, Fig. S3 *A–C*). In Hela cells, the ectopically expressed GFP-PRMT3 colocalized with ectopically expressed cGAS, RIG-I, and MDA5, respectively (*SI Appendix*, Fig. S3*D*). Subsequent domain mapping indicated that the helicase domain of RIG-I or MDA5 mainly bound to PRMT3 (*SI Appendix*, Fig. S4 *A–D*), the RD domain of cGAS primarily associated with PRMT3 (*SI Appendix*, Fig. S5 *A* and *B*). Additionally, the catalytic core domain of PRMT3 exhibited primary binding affinity toward cGAS (*SI Appendix*, Fig. S5 *C* and *D*). In THP-1 cells, endogenous PRMT3 was also coimmunoprecipitated with endogenous RIG-1, MDA5, or cGAS with or without SeV or HSV-1 infection (Fig. 5 *B* and *C*). Strikingly, SeV infection led to a gradual decrease of RIG-I and MDA5 pulled down by PRMT3 (Fig. 5*B*), and HSV-1 infection resulted in a progressively decreased association of PRMT3 and cGAS (Fig. 5*C*). Furthermore, using a specific antibody against the asymmetric dimethylation of arginine (Asym24), we observed a progressive reduction in arginine asymmetric dimethylation of RIG-I, MDA5, and cGAS after being infected with VSV, EMCV, and HSV-1, respectively (Fig. 5 *D–F*).

Subsequently, we examined whether PRMT3 could catalyze asymmetric arginine dimethylation of RIG-I, MDA5, and cGAS. As expected, the wild-type PRMT3 catalyzed asymmetric arginine dimethylation of RIG-I, MDA5, and cGAS efficiently, but the enzymatically inactive mutant, PRMT3-3M, failed to exhibit such an activity (Fig. 5 *G–I*). In addition, treatment with SGC707 suppressed asymmetric arginine dimethylation of RIG-I, MDA5, and cGAS effectively (Fig. 5 *G–I*).

Next, we utilized *Prmt3*$^{+/+}$ and *Prmt3*$^{-/-}$ MLFs to determine the effect of endogenous Prmt3 on the endogenous asymmetric dimethylation of Mda5, Rig-I, and cGas. In response to poly (I:C) transfection, VSV or HSV-I infection, asymmetric arginine dimethylation of Mda5, Rig-I, or cGas was higher in *Prmt3*$^{+/+}$ MLFs than in *Prmt3*$^{-/-}$ MLFs (Fig. 5 *J–L*), which was progressively decreased along with time of transfection or infection (Fig. 5 *J–L*). Moreover, asymmetric arginine dimethylation of RIG-I, MDA5, and cGAS in the lungs of *Prmt3*$^{+/-}$ mice was significantly reduced compared with that in lungs of *Prmt3*$^{+/+}$ mice (*SI Appendix*, Fig. S6).

To further validate that cGAS in the cGAS–STING pathway was specifically targeted by PRMT3, we performed the cGAMP assay. As shown in *SI Appendix*, Fig. S7, the cGAMP activity was significantly higher in *Prmt3*$^{-/-}$ MEFs than that in *Prmt3*$^{+/+}$ MEFs after transfection of ISD45. Thus, Prmt3 targets cGAS rather than STING in the cGAS–STING pathway.

These data suggest that PRMT3 targets cytosolic RNA sensors RIG-I and MDA5 as well as DNA sensor cGAS, to catalyze their asymmetric arginine dimethylation.

PRMT3 Inhibits the RNA-Binding Ability of RIG-I and MDA5 by Catalyzing Asymmetric Dimethylation of RIG-I on Arginine 730 (R730) and MDA5 on Arginine 822 (R822), Respectively. PRMT3 can interact and catalyze asymmetric arginine dimethylation of both RIG-I and MDA5, which have an intensively conserved domain structure, and domain mapping also suggests that both RIG-I and MDA5 rely on their helicase domain to bind to PRMT3. We thus speculated that PRMT3 might target the conserved arginine residue(s) between RIG-I and MDA5. After comparing the amino acid sequences of human and mouse MDA5 and RIG-I, we noticed that six arginine residues are evolutionarily conserved between human and mouse MDA5 and RIG-I (*SI Appendix*, Fig. S8*A*). Subsequently, we mutated these arginine residues in RIG-I and MDA5 to lysine residues, respectively. Initially, we compared the induction ability of these mutants on the activity of the IFN-β promoter reporter and ISRE reporter. In response to stimulation with 5′ppp-dsRNA, overexpression of RIG-I mutants, R244K, R546K, R637K, R728K, and R732K, promoted the activity of the IFN-β promoter reporter and ISRE reporter similar to that of the wild-type RIG-I (Fig. 6*A* and *SI Appendix*, Fig. S8*B*). However, overexpression of the RIG-I mutant, R730K, significantly enhanced the activity of the IFN-β promoter reporter and the ISRE reporter compared with overexpression of wild-type RIG-I (Fig. 6*A* and *SI Appendix*, Fig. S8*B*), implicating that R730 is a potential methylation site on RIG-I. Interestingly, overexpression of the MDA5 mutant, R822K, also significantly enhanced the activity of the IFN-β promoter reporter and ISRE reporter compared with the overexpression of wild-type MDA5 (Fig. 6*B* and *SI Appendix*, Fig. S8*C*). To validate these potential arginine dimethylation sites in RIG-I and MDA5, we performed an in vitro methylation assay. The results showed that wild-type PRMT3, but not PRMT3-3M, directly catalyzed the asymmetric arginine dimethylation of the helicase domain of RIG-I and MDA5 (Fig. 6 *C* and *D*). Notably, the mutant forms RIG-I-R730K and MDA5-R822K failed to undergo methylation by PRMT3 (Fig. 6 *C* and *D*). Furthermore, through mass spectrometry analyses, we identified that the residue R822 in MDA5 was susceptible to methylation in the presence of PRMT3 overexpression (*SI Appendix*, Fig. S8*D*). We next confirmed that overexpression of RIG-I-R730K or MDA5-R822K caused an increase of *IFNB1* mRNA higher than that of wild-type RIG-I or MDA5 in response to VSV infection or poly (I:C) transfection, respectively (Fig. 6 *E* and *F*). Moreover, upon VSV infection or poly (I:C) transfection, phosphorylation of TBK1 (p-TBK1) and IRF3 (p-IRF3) induced by RIG-I-R730K or MDA5-R822K was higher than that by the wild-type RIG-I (RIG-I-WT) or MDA5 (MDA5-WT) respectively (Fig. 6 *G* and *H*). Notably, R730 of RIG-I and R822 of MDA5 are evolutionarily conserved between human and mouse MDA5 and RIG-I (*SI Appendix*, Fig. S8*A*),

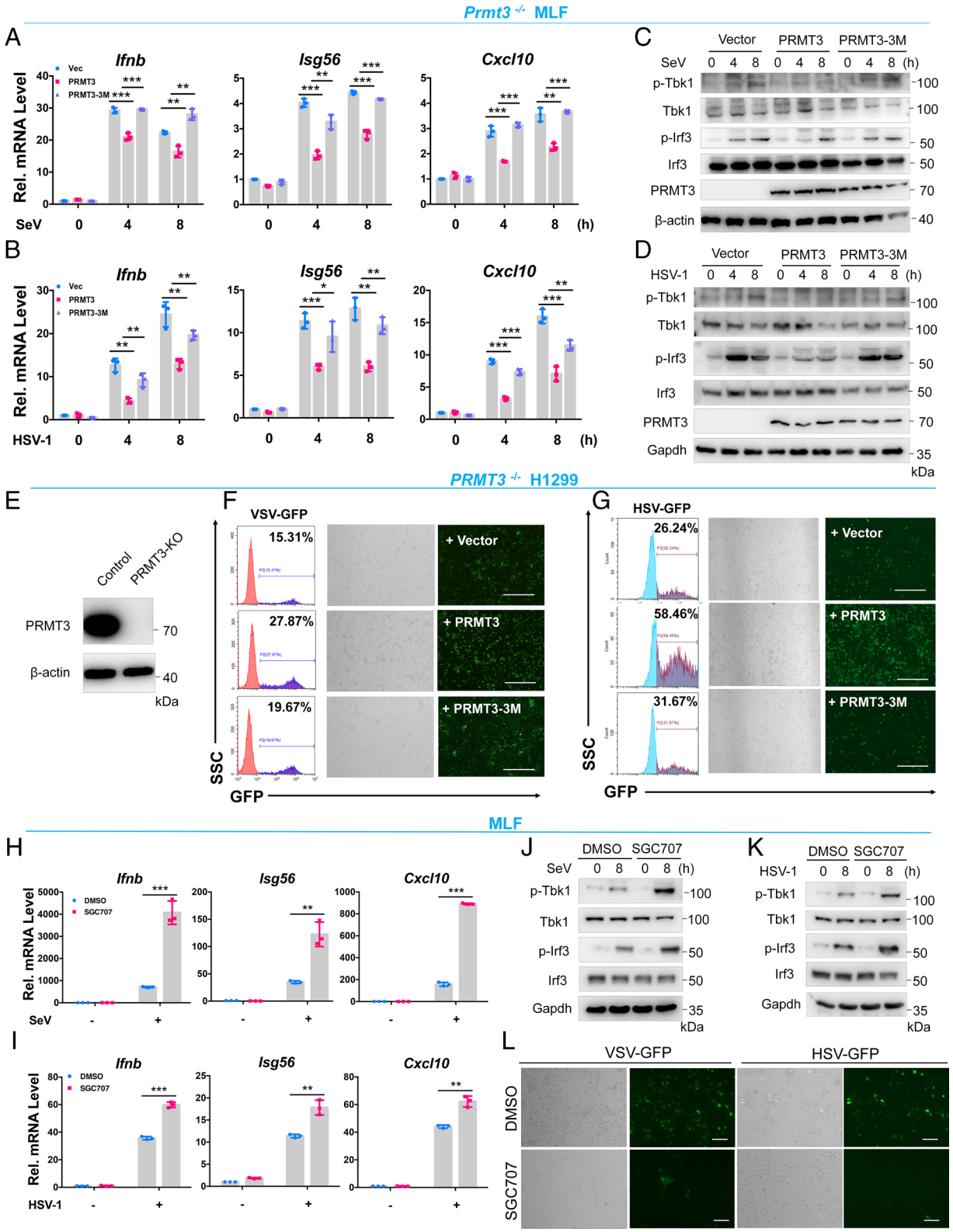

Fig. 4. PRMT3 attenuates antiviral innate immune response via its methyltransferase activity. (*A* and *B*) qRT-PCR analysis of *Ifnb1, Isg56, Cxcl10* mRNA in *Prmt3*$^{-/-}$ MLFs stably expressing empty vector (Vec), PRMT3, or the enzymatically inactive mutant PRMT3-3M (G263A/C264A/G265A) followed by infection with SeV (*A*) or HSV-1 (*B*) for 0 to 8 h. (*C* and *D*) Phosphorylation of Tbk1 and Irf3 in *Prmt3*$^{-/-}$ MLFs stably expressing empty vector (Vec), PRMT3, or the enzymatically inactive mutant PRMT3-3M with SeV (*C*) or HSV-1 (*D*) infection for 0 to 8 h. (*E*) IB analysis of PRMT3 in WT (*PRMT3*$^{+/+}$) and *PRMT3*$^{-/-}$ H1299 cells. (*F* and *G*) Flow cytometry analysis (left graphs) and microscopy imaging (right images) of the replication of VSV-GFP (*F*) and HSV-GFP (*G*) in *PRMT3*$^{-/-}$ H1299 cells transfected with the indicated plasmids, followed by VSV-GFP (1 MOI) or HSV-GFP (1 MOI) challenge for 12 h, the numbers adjacent to the outlined areas indicate percentages of GFP-positive H1299 cells. (Scale bar, 500 μm.) (*H* and *I*) qRT-PCR analysis of *Ifnb1, Isg56, Cxcl10* mRNA in MLFs pretreated with either DMSO or SGC707 (1 μM) for 16 h, followed with or without SeV (*H*) or HSV-1 (*I*) infection for 8 h. (*J* and *K*) Phosphorylation of Tbk1 and Irf3 in MLFs pretreated with either DMSO or SGC707 (1 μM) for 16 h, followed with or without SeV (*J*) or HSV-1 (*K*) infection for 8 h. (*L*) Microscopy imaging of the replication of VSV-GFP (*Left*) and HSV-GFP (*Right*) in MLFs pretreated with either DMSO or SGC707 (1 μM) for 16 h, followed by VSV-GFP (1 MOI) or HSV-GFP (1 MOI) challenge for 12 h. (Scale bar, 100 μm.) **P* < 0.05, ***P* < 0.01, and ****P* < 0.001, using two-way ANOVA with Holm–Sidak's multiple comparisons test (*A, B, H,* and *I*). Data are representative of three independent experiments (*A, B, H,* and *I*; mean ± SD of three technical replicates) or represent two independent experiments (*C–G* and *J–L*).

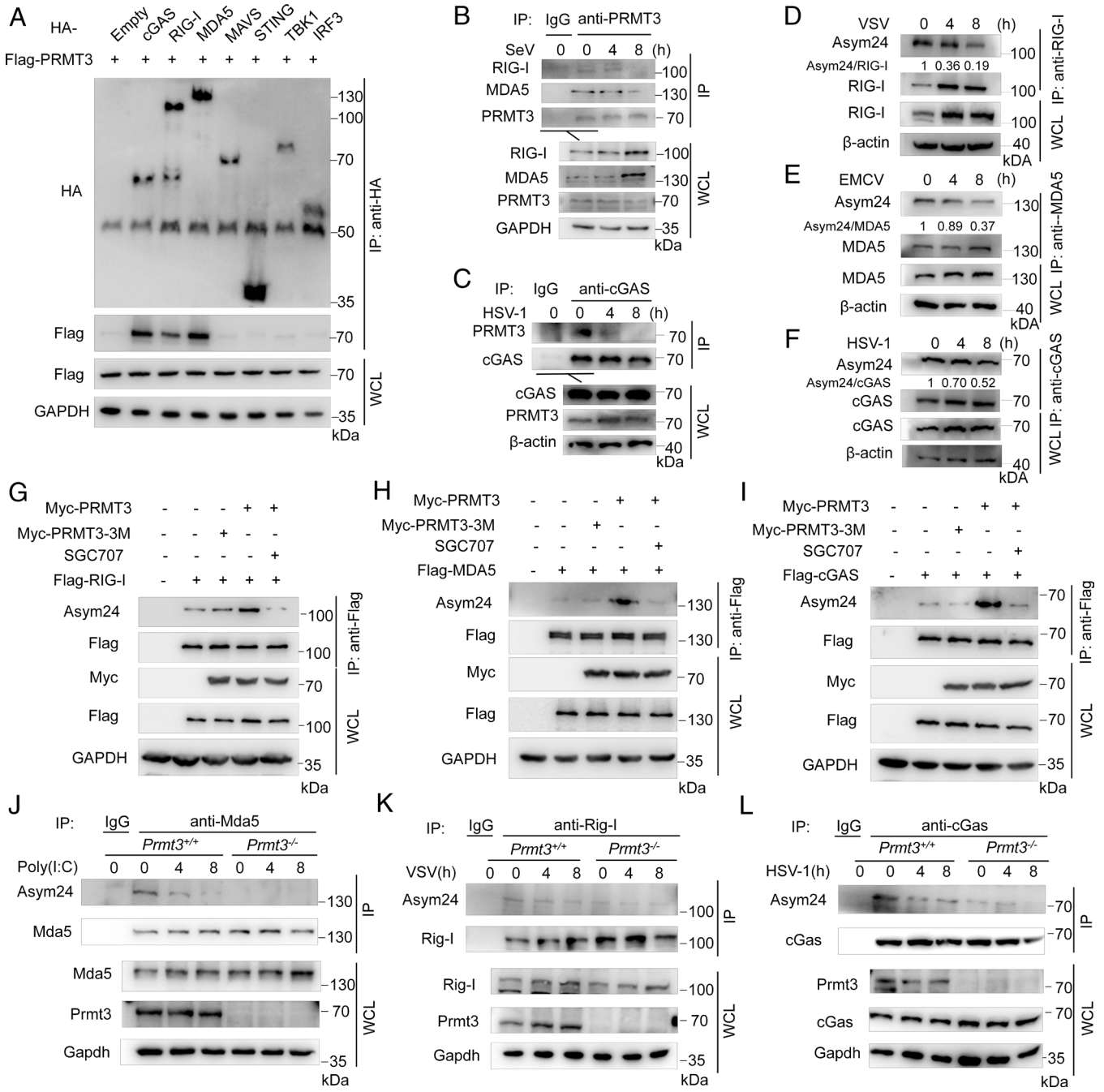

Fig. 5. PRMT3 catalyzes asymmetric arginine dimethylation of cytosolic RNA sensors RIG-I and MDA5 as well as DNA sensor cGAS. (*A*) IB of whole-cell lysates (*Bottom*) and proteins immunoprecipitated with anti-HA antibody–conjugated agarose beads (*Top*) from HEK293T cells transfected with the indicated plasmids for 24 h. (*B*) IB of whole-cell lysates (*Bottom*) and proteins immunoprecipitated with anti-PRMT3 antibody (*Top*) from THP-1 cells left uninfected or infected with SeV for 0 to 8 h. (*C*) IB of whole-cell lysates (*Bottom*) and proteins immunoprecipitated with anti-cGAS antibody (*Top*) from THP-1 cells left uninfected or infected with HSV-1 for 0 to 8 h. (*D–F*) Endogenous arginine asymmetric dimethylation of RIG-I (*D*), MDA5 (*E*), or cGAS (*F*) in THP-1 cells infected with VSV or EMCV or HSV-1 for 0 to 8 h. (*G–I*) Co-IP analysis of arginine asymmetric dimethylation of Flag-RIG-I (*G*), Flag-MDA5 (*H*), or Flag-cGAS (*I*) in HEK293T cells transfected with Flag-RIG-I or Flag-MDA5 and Myc-PRMT3 or its catalytic mutant (Myc-PRMT3-3M) and then pretreated with or without SGC707 for 16 h. (*J–L*) Endogenous arginine asymmetric dimethylation of RIG-I (*J*), MDA5 (*K*), or cGAS (*L*) in *Prmt3*$^{+/+}$ and *Prmt3*$^{-/-}$ MLFs transfected with Poly(I:C) or infected with VSV or HSV-1 for 0 to 8 h. WCL, whole cell lysate; IP, immunoprecipitation. Data are representative of three independent experiments.

which are also located in the RGG/RG motif, the most common amino acid sequences favored by PRMTs (45). Altogether, these data suggest that PRMT3 might inhibit RNA-induced interferon response mainly by targeting RIG-I on R730 and MDA5 on R822, respectively, to catalyze their asymmetric dimethylation.

Activation of the RLR signaling is initiated by RIG-I or MDA5 binding to viral RNAs (2). The influence on the RNA-binding ability of RIG-I and MDA5 can directly affect their subsequent activation (1). Considering that R730 of RIG-I and R822 of MDA5 targeted by PRMT3 are both located in their helicase domains, which are responsible for RNA binding (46), we thus examined whether PRMT3 can affect the RNA-binding ability of RIG-I and MDA5. The in vitro pull-down assay for RNA binding indicated that both RIG-I and MDA5 bound to more RNA in *PRMT3*$^{-/-}$ H1299 cells than in *PRMT3*$^{+/+}$ H1299 cells (Fig. 6 *I* and *J*). Consistently, treatment with the PRMT3 inhibitor,

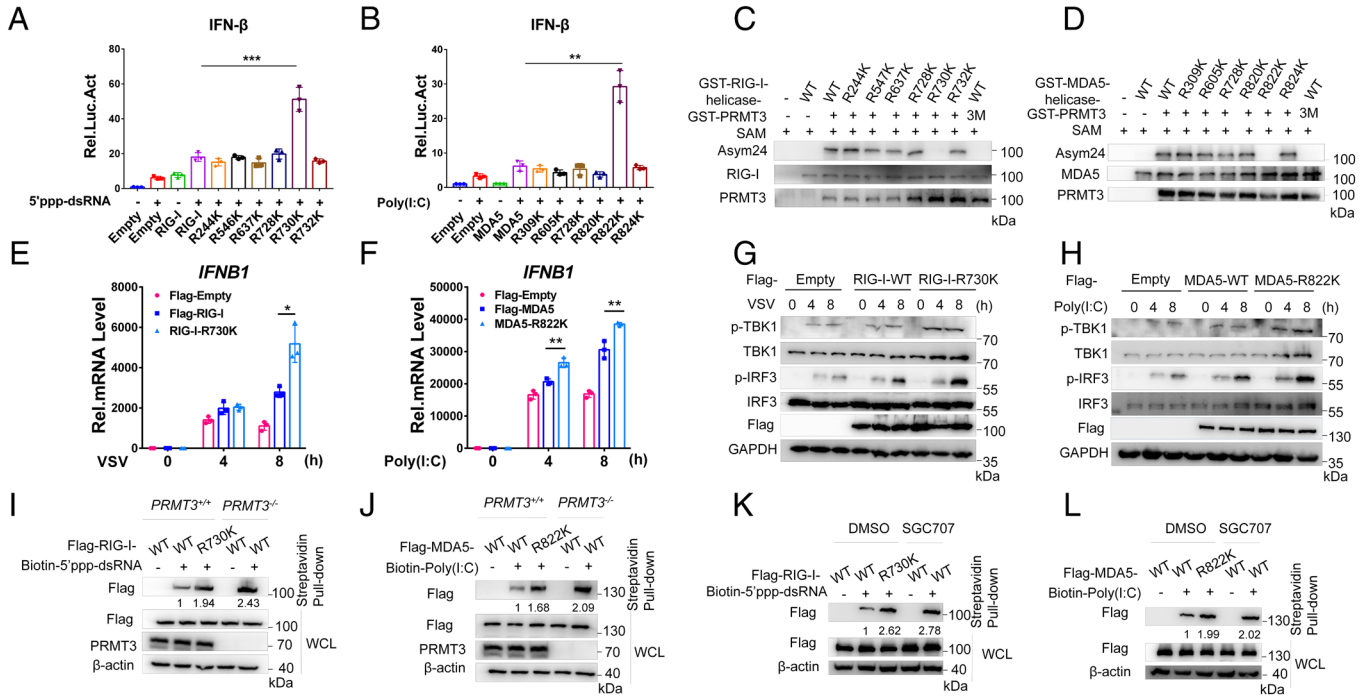

Fig. 6. Asymmetric arginine dimethylation of RIG-I and MDA5 mediated by PRMT3 inhibits their RNA-binding ability. (*A* and *B*) Luciferase activity of IFN-β in H1299 cells transfected with the indicated plasmids for 16 h, followed by transfection of 5′ppp-dsRNA (*A*) or poly(I:C) (*B*) for 8 h before luciferase assays. (*C* and *D*) In vitro methylation analysis of bacterially expressed GST-tagged-RIG-I-helicase or its arginine-to-lysine substitution mutants (*C*), and bacterially expressed GST-tagged-MDA1-helicase or its arginine-to-lysine substitution mutants (*D*), in the presence of S-adenosylmethionine (SAM) and GST-tagged-PRMT3 or its catalytic mutant (GST-PRMT3-3M). (*E* and *F*) qRT-PCR analysis of IFNB1 mRNA in H1299 cells transfected with the indicated plasmids, followed by VSV infection (*E*) or poly(I:C) transfection (*F*) for 0 to 8 h. (*G* and *H*) Phosphorylation of TBK1 and IRF3 in H1299 cells transfected with the indicated plasmids followed by VSV infection (*G*) or poly(I:C) (*H*) transfection for 0 to 8 h. (*I* and *J*) RNA-binding assay of RIG-I (*I*) and MDA5 (*J*) or their arginine-to-lysine substitution mutants, RIG-I-R730K (*I*) and MDA5-R822K (*J*). PRMT3-KO ($PRMT3^{-/-}$) and control ($PRMT3^{+/+}$) H1299 cells were transfected with Flag-RIG-I-WT or Flag-RIG-I-R730K (*I*), and Flag-MDA5-WT or Flag-MDA5-R822K (*J*). Twenty hours after transfection, cell lysates were incubated with biotinylated-5′ppp-dsRNA or biotinylated-poly(I:C) and streptavidin–Sepharose. Bound proteins were analyzed by immunoblots with anti-Flag antibody. (*K* and *L*) RNA-binding assay of RIG-I (*K*) and MDA5 (*L*) or their arginine-to-lysine substitution mutants, RIG-I-R730K (*K*) and MDA5-R822K (*L*) in the presence of DMSO control or SGC707. H1299 cells were pretreated with DMSO or SGC707 for 16 h, followed by transfection of Flag-RIG-I or its arginine-to-lysine substitution mutant, RIG-I-R730K (*K*) and Flag-MDA5-WT or Flag-MDA5-R822K (*L*). Twenty hours after transfection, cell lysates were incubated with biotinylated-5′ppp-dsRNA or biotinylated-poly(I:C) and streptavidin–Sepharose. Bound proteins were analyzed by immunoblots with anti-Flag antibody. $*P < 0.05$, $**P < 0.01$, and $***P < 0.001$, using unpaired Student's *t* test (*A* and *B*) or two-way ANOVA with Holm–Sidak's multiple comparisons test (*E* and *F*). Data are representative of three independent experiments (*A, B, E,* and *F*; mean ± SD of three technical replicates) or represent two independent experiments (*C, D,* and *G–L*).

SGC707, enhanced RNA binding to RIG-I and MDA5 (Fig. 6 *K* and *L*). Furthermore, RIG-I-R730K and MDA5-R822K exhibited enhanced RNA-binding ability compared to the wild-type RIG-I and MDA5 (Fig. 6 *I–L*).

Taken together, these data suggest that PRMT3 targets Arginine 730 (R730) of RIG-I and Arginine 822 (R822) of MDA5 for asymmetric dimethylation, leading to the inhibition of their RNA-binding ability.

PRMT3 Inhibits the DNA-Binding Ability and Oligomerization of cGAS by Catalyzing Asymmetric Dimethylation of cGAS on Arginine 111 (R111). In this study, we identify that PRMT3 interacts with the N terminus of cGAS (*SI Appendix*, Fig. S5 *A* and *B*). However, we noticed that the N terminus of cGAS was not so evolutionarily conserved. To determine which arginine residue(s) of cGAS is (are) targeted by PRMT3 for asymmetric dimethylation, we turned to utilize mass spectrometry. Arginine 60 (R60) and arginine 111 (R111) in human cGAS were identified to be methylated when *PRMT3* was overexpressed (*SI Appendix*, Fig. S9 *A* and *B*).

Subsequently, we constructed two arginine methylation-deficient mutants of cGAS, cGAS-R60K, and cGAS-R111K, respectively, and examined their behaviors. The in vitro methylation assay showed that PRMT3 directly catalyzed cGAS asymmetric arginine dimethylation and, cGAS-R111K, rather than cGAS-R60K, failed to be methylated by PRMT3 (Fig. 7*A*), which indicates that R111 of cGAS is the methylation sites targeted by PRMT3. Notably, R92 of mouse cGas, identical to R111 of Human cGAS, was also identified to be methylated by mass spectrometry when *Prmt3* was overexpressed (*SI Appendix*, Fig. S9 *C* and *D*). Furthermore, upon transfection of poly(dA:dT), a mimic of dsDNA, overexpression of cGAS-R111K, but not overexpression of cGAS-R60K, together with STING increased the activity of the IFN-β promoter reporter significantly compared with overexpression of the wild-type cGAS together with STING (Fig. 7*B*). Upon stimulation with poly(dA:dT), the induction of *IFNB1* mRNA in H1299 cells by overexpression of cGAS-R111K was higher than that by overexpression of the wild-type cGAS (Fig. 7*C*). Consistently, upon stimulation with poly(dA:dT), p-TBK1 and p-IRF3 induced by overexpression of cGAS-R111K were higher than that by overexpression of the wild-type cGAS (cGAS-WT) (Fig. 7*D*). Taken together, these data suggest that PRMT3 inhibits DNA-induced interferon response primarily by targeting cGAS on R111 for asymmetric dimethylation.

cGAS is a dsDNA-activated enzyme, and the minimal functional unit of enzymatically active cGAS is a dimer (7). When activated, cGAS forms an oligomeric complex with DNA and undergoes switch-like conformational changes (47). To further determine how PRMT3 affects cGAS activation, we examined the effects of PRMT3 on the DNA-binding ability and oligomerization of

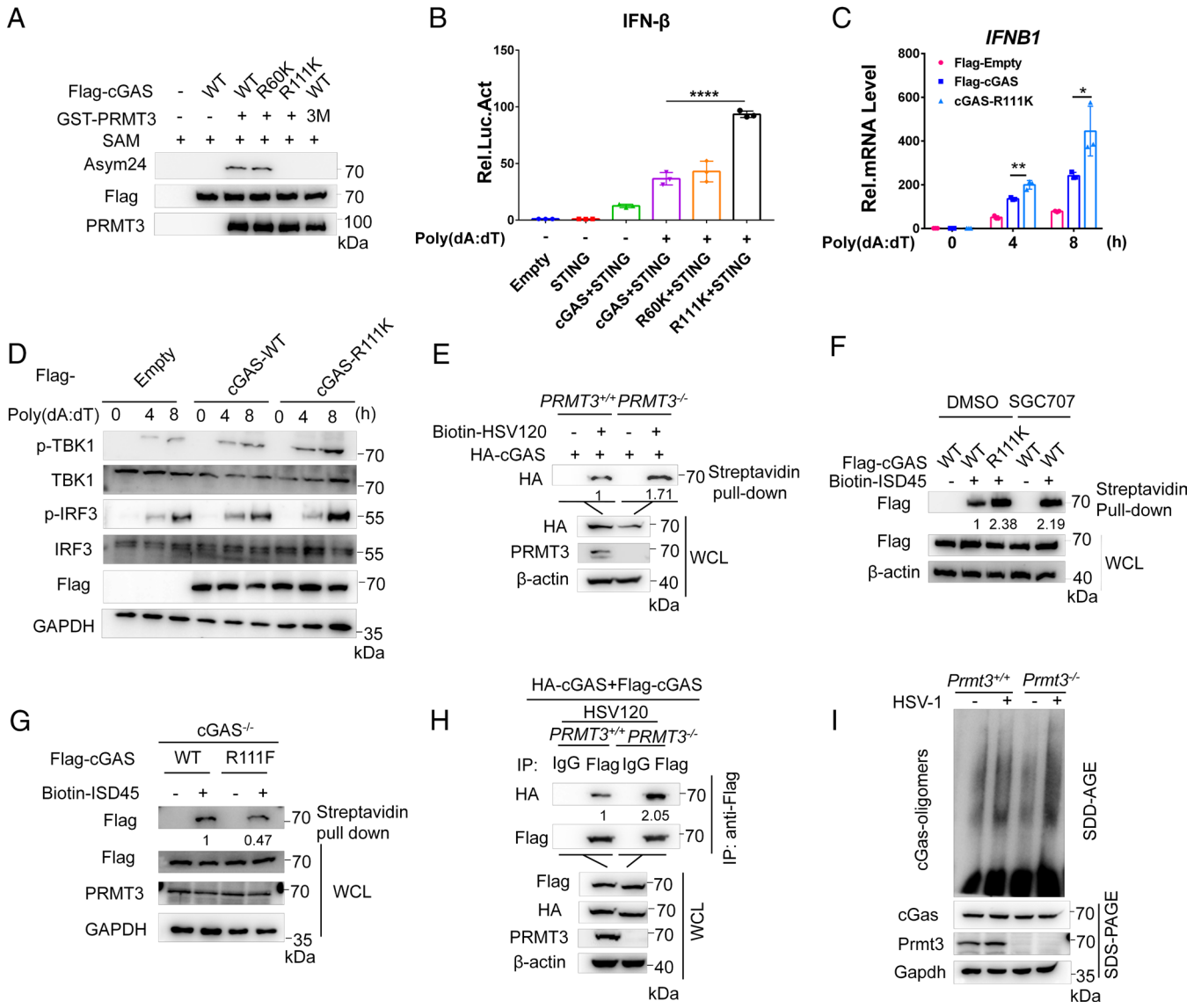

Fig. 7. Asymmetric arginine dimethylation of cGAS mediated by PRMT3 inhibits its DNA-binding ability. (*A*) In vitro methylation analysis of purified Flag-cGAS or its arginine-to-lysine substitution mutants in the presence of S-adenosylmethionine (SAM) and GST-tagged-PRMT3 or its catalytic mutant (GST-PRMT3-3M). (*B*) Luciferase activity of IFN-β in H1299 cells transfected with the indicated plasmids for 16 h, followed by transfection of poly (dA:dT) for 8 h before luciferase assays. (*C*) qRT-PCR analysis of *IFNB1* mRNA in H1299 cells transfected with the indicated plasmids, followed by poly (dA:dT) transfection for 0 to 8 h. (*D*) Phosphorylation of TBK1 and IRF3 in H1299 cells transfected with the indicated plasmids followed by poly (dA:dT) transfection for 0 to 8 h. (*E*) *PRMT3* deficiency enhances the binding ability of cGAS to DNA. PRMT3-KO (*PRMT3*$^{-/-}$) and control (*PRMT3*$^{+/+}$) H1299 cells were transfected with HA-cGAS. Twenty hours after transfection, cell lysates were incubated with biotinylated-HSV120 and streptavidin–Sepharose. Bound proteins were analyzed by immunoblots with anti-HA antibody. (*F*) DNA-binding assay of cGAS or its arginine-to-lysine substitution mutants, cGAS-R111K in the presence of DMSO control or SGC707. H1299 cells were pretreated with DMSO or SGC707 for 16 h, followed by transfection of Flag-cGAS or its arginine-to-lysine substitution mutant, Flag-cGAS-R111K. Twenty hours after transfection, cell lysates were incubated with biotinylated-ISD45 and streptavidin–Sepharose. Bound proteins were analyzed by immunoblots with anti-Flag antibody. (*G*) DNA-binding assay of cGAS with its methyl-mimic mutant, cGAS-R111F. cGAS-KO H1299 cells (*cGAS*$^{-/-}$) were transfected with Flag-cGAS-WT or Flag-RIG-I-R111F. Twenty hours after transfection, cell lysates were incubated with biotinylated-HSV120 and streptavidin–Sepharose. Bound proteins were analyzed by immunoblots with anti-Flag antibody. (*H*) Effects of PRMT3-deficiency on self-association of cGAS. *PRMT3*-KO (*PRMT3*$^{-/-}$) and control (*PRMT3*$^{+/+}$) H1299 cells were transfected with the indicated plasmids for 20 h before coimmunoprecipitation and immunoblotting analysis with the indicated antibodies. (*I*) Effects of PRMT3-deficiency on oligomerization of cGAS induced by HSV-1 infection. *Prmt3*$^{+/+}$ and *Prmt3*$^{-/-}$ MEFs were left uninfected or infected with HSV-1 for 8 h. Cell lysates were then fractionated by SDD-AGE and SDS-PAGE and analyzed by immunoblotting with the indicated antibodies. *$P < 0.05$, **$P < 0.01$, and ****$P < 0.001$, using unpaired Student's *t* test (*B*) or two-way ANOVA with Holm–Sidak's multiple comparisons test (*C*). Data are representative of three independent experiments (*B* and *C*; mean ± SD of three technical replicates) or represent two independent experiments (*A* and *D*–*I*).

cGAS. In *PRMT3*$^{-/-}$ H1299 cells, the binding of cGAS to the DNA HSV120 is obviously higher than that in *PRMT3*$^{+/+}$ H1299 cells (Fig. 7*E*). Compared with wild-type cGAS, cGAS-R111K exhibited an enhanced DNA ISD45 binding ability (Fig. 7*F*). Similarly, treatment with SGC707 also enhanced the binding of cGAS to DNA ISD45 (Fig. 7*F*). By contrast, the reconstituted cGAS-R111F, an arginine methylation-mimic mutant of cGAS, bound to less DNA ISD45 than the reconstituted wild-type cGAS (WT) (Fig. 7*G*). In addition, HSV120-stimulated self-association of cGAS was obviously enhanced in *PRMT3*$^{-/-}$ H1299 cells compared with that in *PRMT3*$^{+/+}$ H1299 cells (Fig. 7*H*). Moreover, HSV-1 stimulated oligomerization of cGAS was promoted in *Prmt3*$^{-/-}$ MEFs compared with that in *Prmt3*$^{+/+}$ MEFs (Fig. 7*I*).

These data suggested that PRMT3 targets R111 of cGAS to catalyze asymmetric dimethylation, leading to the inhibition of the DNA-binding ability and oligomerization of cGAS.

Based on the above observations, we proposed a working model for PRMT3 in antiviral innate immunity (*SI Appendix*, Fig. S10).

Discussion

In our previous study, we found that zebrafish *prmt3* negatively regulates antiviral innate immunity in response to RNA virus infection (26). In this study, using a mammalian system, we not only revealed that PRMT3 attenuates antiviral innate immunity in response to RNA virus infection through catalyzing asymmetric arginine dimethylation of cytosolic viral RNA sensors, RIG-I and MDA5, but also revealed that PRMT3 attenuates antiviral innate immunity in response to DNA virus infection through catalyzing asymmetric arginine dimethylation of cytosolic viral DNA sensor, cGAS. To keep efficient immune response to viral infection and simultaneously avoid autoimmune pathogenesis, organisms must accurately control antiviral innate immunity to balance the activation and suppression of innate immune response (1, 27, 48, 49). Serving as the initiation molecules of type I IFN signaling, the cytosolic nucleic acid sensors binding to RNA or DNA derived from either invading pathogens or endogenous to the cell initiate the signaling (49). Here, we identified that PRMT3 catalyzes asymmetric arginine dimethylation of RIG-I, MDA5, and cGAS, leading to the suppression of RIG-I and MDA5 binding to RNA, as well as cGAS binding to DNA. Considering that PRMT3 interacts with and methylates RIG-I, MDA5, and cGAS even without virus infection, PRMT3 might thus respond for avoiding excessive activation of innate immunity in resting states through preventing the cytosolic nucleic acid sensors to bind to cellular endogenous RNA or DNA. In fact, we noticed that with the prolongation of virus infection, PRMT3 binding to RIG-I, MDA5, and cGAS, as well as the asymmetric arginine dimethylation of RIG-I, MDA5, and cGAS by PRMT3, was getting weaker and weaker, indicating that a negative feedback mechanism exists for releasing the suppressive role of PRMT3 on antiviral immune response during viral infection. Intriguingly, a human gain of function mutation in R822 of MDA5, R822Q, causes Singleton–Merten syndrome exhibiting with excessive IFN-β induction, which highlights the importance of R822 of MDA5 in the RLR signaling identified in this study (50).

Arginine methylation increases steric hindrance by adding a bulky group and eliminates preexisting hydrogen bonds with surrounding amino acid residues, which is involved in many physiological processes by modulating protein–protein interactions (45). Notably, it appears that the most of PRMTs positively or negatively regulate type I IFN signaling at multiple levels of type I IFN signaling through different mechanisms (24–31). In this study, we identified that PRMT3 directly methylates both cytosolic RNA and DNA sensors, resulting in the suppression of IFN signaling, which not only adds to complexity but also reinforces the functional importance of arginine methylation in the regulation of type I IFN signaling.

Given that the enzymatic activity of PRMT3 is of vital importance in inhibiting type I IFN signaling, the specific inhibitor of PRMT3 might be developed as a therapeutic drug for the treatment of virus infection. Of note, it seems that the methyltransferase activity of all PRMTs studied so far is essential for acting their roles in antiviral immune response. However, due to the opposite effects acted by different PRMTs in type I IFN signaling, it must concern seriously when planning to develop their inhibitors as therapeutic drugs.

It seems that the inhibitory role of PRMT3 in type I IFN signaling is released along with virus infection. However, the underlying mechanism remains to be elucidated. Similar to the most protein modifications, arginine methylation is supposed to be dynamic modifications. But, to date, it is barely known about arginine demethylation. So, it remains enigmatic whether arginine demethylase or other modifications are involved in this process. Of note, in addition to arginine methylation, multiple other modifications can also regulate the activation of cytosolic RNA and DNA sensors. To further define how much of PRMT3-mediated arginine methylation contributes to the regulation of these sensors' activation will give mechanistic insights into the regulation of type I IFN signaling.

Materials and Methods

The following is a brief description of Materials and Methods, and the description of Materials and Methods in detail is provided in *SI Appendix*

Mice. All animal works were carried out in accordance with the NIH Guide for the Care and Use of Laboratory Animals, and all the animal protocols used in this study have been approved by IACUC (Institutional Animal Care and Use Committee) of Institute of Hydrobiology, Chinese Academy of Sciences.

CRISPR-Cas9 Knockout Cell Lines. Double-stranded oligonucleotides corresponding to the target sequences were cloned into the LentiCRISPRv2 plasmid and then cotransfected with viral packaging plasmids into HEK293T cells.

In Vitro Pull-Down Assay. Poly(I:C) and 5′ppp-dsRNA were conjugated with biotin by UV (365-nm wavelength) cross-linking. HEK293T cells transfected with the indicated plasmids were lysed in NP-40 lysis buffer. Lysates were incubated with biotinylated-poly(I:C), biotinylated-5′ppp-dsRNA, biotinylated-ISD45, or biotinylated-HSV120 (Tsingke Biotech) and then incubated with streptavidin beads.

In vitro Methylation Assays. For In Vitro methylation of cGAS, briefly, Flag-cGAS or its mutants expressed in HEK293T cells were immunoprecipitated with anti-Flag antibody–conjugated agarose beads. After washing, the beads were directly incubated with bacterially expressed GST-PRMT3 WT or 3M. For in vitro methylation of the helicase domain of RIG-I and MDA5, bacterially expressed GST-PRMT3 WT or 3M were incubated with bacterially expressed GST-RIG-I-helicase or GST-MDA5-helicase, respectively.

Semidenaturing Detergent Agarose Gel Electrophoresis (SDD-AGE). MEFs were lysed in NP-40 lysis buffer, and the cell lysates were mixed in 1× sample buffer (0.5× TBE, 10% glycerol, 2% SDS, and 0.0025% bromophenol blue) and loaded onto a vertical 2% agarose gel.

cGAMP Assay. MEFs (1×10^7) transfected with dsDNA were harvested and homogenized. The homogenates were heated at 95 °C for 10 min followed by centrifuge at 15,000 rpm for 2 h. The supernatants (900 μL) were mixed with 10 × digitonin (100 μL) and incubated with HFFs (1×10^6). After 30 min, the supernatants were removed and full medium was added to HFFs for 4 h followed by qRT-PCR assays.

Identification of MDA5 and cGAS Methylated Arginine Site(s) by Mass Spectrometry. HEK293T cells were transfected with human or mouse Flag-cGAS and Myc-PRMT3, or human Flag-MDA5 and Myc-PRMT3. Cell lysate was immunoprecipitated with anti-Flag antibody–conjugated agarose beads overnight. Immunoprecipitated cGAS or MDA5 were subjected to 8% SDS-PAGE gel. After Coomassie Brilliant Blue staining, we excised the band corresponding to the cGAS or MDA5. Subsequently, the purified proteins were digested by trypsin and analyzed by online nanoflow LC-MS/MS using the Ultimate 3000 nano-LC system (Dionex) connected to an LTQ-Orbitrap Elite (Thermo Fisher Scientific) mass spectrometer.

Lentivirus-Mediated Gene Transfer. HEK293T cells were transfected with phage-PRMT3, phage-PRMT3-3M, or the empty vector along with the packaging vectors pSPAX2 and pMD2G. The medium was changed for fresh full medium and then harvested for cell infection.

Viral Infection in Cells and Mice. Cells were seeded into 24-well plates (2×10^5 cells/per well) or six-well plates (10^6 to 10^7 cells/per well). After 24 h, cells were infected with SeV, VSV, VSV-GFP, EMCV, MCMV, ECTV, HSV-1, or HSV-GFP. The cells were collected for qRT-PCR or immunoblot assays. For mice infection, SGC707 (30 mg/kg) was administered by i.p. injection 24 h before viral infection. Six- to eight-week-old and sex-matched (male) $Prmt3^{+/+}$ and $Prmt3^{+/-}$ littermates were intraperitoneally injected with EMCV (1×10^6 PFU/per mouse) or HSV-1 (1×10^7 PFU/per mouse).

Viral Titer Determination. For viral titer determination in infected cells, the indicated cells were infected with VSV or HSV-1. For viral titer determination in mice, *Prmt3*$^{+/+}$ and *Prmt3*$^{+/-}$ mice were intraperitoneally injected with EMCV (1×10^6 PFU/per mouse) or HSV-1 (1×10^7 PFU/per mouse) for 24 h, the homogenates of lungs, livers, or spleens were collected for viral titer determination.

Statistical Analysis. Differences between experimental and control groups were determined by Student's *t* test or by two-way ANOVA. For the mouse survival study, Kaplan–Meier survival curves were generated and analyzed by the log-rank test. Statistical analyses were performed using GraphPad Prism 6 software. ns, not significant ($P > 0.05$); *$P < 0.05$; **$P < 0.01$; ***$P < 0.001$.

Data, Materials, and Software Availability. All study data are included in the article and/or *SI Appendix*.

ACKNOWLEDGMENTS. We thank Cyagen Biosciences Inc. (Guangzhou, China) for assistance with generation of *prmt3*-deficienct mice. We thank Drs. Hongbing Shu, Bo Zhong, Mingzhou Chen, Chunfu Zheng, and Hong Tang for providing reagents. We thank Yan Wang and Fang Zhou at the Core Facility of Institute of Hydrobiology for FACS and the confocal microscope. This work was supported by grants from the National Natural Science Foundation of China (31830101 and 31721005), the Strategic Priority Research Program of the Chinese Academy of Sciences (XDA24010308), and the National Key Research and Development Program of China (2018YFD0900602).

1. X. Tan, L. Sun, J. Chen, Z. J. Chen, Detection of microbial infections through innate immune sensing of nucleic acids. *Annu. Rev. Microbiol.* **72**, 447–478 (2018).
2. A. Ablasser, S. Hur, Regulation of cGAS- and RLR-mediated immunity to nucleic acids. *Nat. Immunol.* **21**, 17–29 (2020).
3. K. P. Hopfner, V. Hornung, Molecular mechanisms and cellular functions of cGAS-STING signalling. *Nat. Rev. Mol. Cell Biol.* **21**, 501–521 (2020).
4. M. Motwani, S. Pesiridis, K. A. Fitzgerald, DNA sensing by the cGAS-STING pathway in health and disease. *Nat. Rev. Genet.* **20**, 657–674 (2019).
5. M. M. Hu, H. B. Shu, Innate immune response to cytoplasmic DNA: Mechanisms and diseases. *Annu. Rev. Immunol.* **38**, 79–98 (2020).
6. K. Kato, H. Omura, R. Ishitani, O. Nureki, Cyclic GMP-AMP as an endogenous second messenger in innate immune signaling by cytosolic DNA. *Annu. Rev. Biochem.* **86**, 541–566 (2017).
7. A. Ablasser *et al.*, cGAS produces a 2′-5′-linked cyclic dinucleotide second messenger that activates STING. *Nature* **498**, 380–384 (2013).
8. H. Kato *et al.*, Differential roles of MDA5 and RIG-I helicases in the recognition of RNA viruses. *Nature* **441**, 101–105 (2006).
9. X. Cai *et al.*, Opposing effects of deubiquitinase OTUD3 in innate immunity against RNA and DNA viruses. *Cell Rep.* **39**, 110920 (2022).
10. V. Hornung *et al.*, 5′-Triphosphate RNA is the ligand for RIG-I. *Science* **314**, 994–997 (2006).
11. A. Pichlmair *et al.*, RIG-I-mediated antiviral responses to single-stranded RNA bearing 5′-phosphates. *Science* **314**, 997–1001 (2006).
12. M. Schlee *et al.*, Recognition of 5′ triphosphate by RIG-I helicase requires short blunt double-stranded RNA as contained in panhandle of negative-strand virus. *Immunity* **31**, 25–34 (2009).
13. M. Yoneyama, T. Fujita, Structural mechanism of RNA recognition by the RIG-I-like receptors. *Immunity* **29**, 178–181 (2008).
14. E. Meylan *et al.*, Cardif is an adaptor protein in the RIG-I antiviral pathway and is targeted by hepatitis C virus. *Nature* **437**, 1167–1172 (2005).
15. L. G. Xu *et al.*, VISA is an adapter protein required for virus-triggered IFN-beta signaling. *Mol. Cell* **19**, 727–740 (2005).
16. T. Kawai *et al.*, IPS-1, an adaptor triggering RIG-I- and Mda5-mediated type I interferon induction. *Nat. Immunol.* **6**, 981–988 (2005).
17. R. B. Seth, L. Sun, C. K. Ea, Z. J. Chen, Identification and characterization of MAVS, a mitochondrial antiviral signaling protein that activates NF-kappaB and IRF 3. *Cell* **122**, 669–682 (2005).
18. M. Yoneyama *et al.*, The RNA helicase RIG-I has an essential function in double-stranded RNA-induced innate antiviral responses. *Nat. Immunol.* **5**, 730–737 (2004).
19. R. S. Blanc, S. Richard, Arginine methylation: The coming of age. *Mol. Cell* **65**, 8–24 (2017).
20. J. Wesche, S. Kuhn, B. M. Kessler, M. Salton, A. Wolf, Protein arginine methylation: A prominent modification and its demethylation. *Cell Mol. Life Sci.* **74**, 3305–3315 (2017).
21. Y. Z. Yang, M. T. Bedford, Protein arginine methyltransferases and cancer. *Nat. Rev. Cancer* **13**, 37–50 (2013).
22. Y. Feng *et al.*, Mammalian protein arginine methyltransferase 7 (PRMT7) specifically targets RXR sites in lysine- and arginine-rich regions. *J. Biol. Chem.* **288**, 37010–37025 (2013).
23. H. Zhang, C. Han, T. Li, N. Li, X. Cao, The methyltransferase PRMT6 attenuates antiviral innate immunity by blocking TBK1-IRF3 signaling. *Cell Mol. Immunol.* **16**, 800–809 (2019).
24. J. Zhu *et al.*, Zebrafish prmt2 attenuates antiviral innate immunity by targeting traf6. *J. Immunol.* **207**, 2570–2580 (2021).
25. J. Zhu *et al.*, Zebrafish prmt7 negatively regulates antiviral responses by suppressing the retinoic acid-inducible gene-I-like receptor signaling. *FASEB J.* **34**, 988–1000 (2020).
26. J. Zhu *et al.*, Zebrafish prmt3 negatively regulates antiviral responses. *FASEB J.* **34**, 10212–10227 (2020).
27. J. J. Zhu *et al.*, Arginine monomethylation by PRMT7 controls MAVS-mediated antiviral innate immunity. *Mol. Cell* **81**, 3171–3186.e8 (2021).
28. Z. Yan *et al.*, The protein arginine methyltransferase PRMT1 promotes TBK1 activation through asymmetric arginine methylation. *Cell Rep.* **36**, 109731 (2021).
29. H. Kim *et al.*, PRMT5 control of cGAS/STING and NLRC5 pathways defines melanoma response to antitumor immunity. *Sci. Transl. Med.* **12**, eaaz5683 (2020).
30. D. Ma *et al.*, Arginine methyltransferase PRMT5 negatively regulates cGAS-mediated antiviral immune response. *Sci. Adv.* **7**, eabc1834 (2021).
31. S. Cui *et al.*, Nuclear cGAS functions non-canonically to enhance antiviral immunity via recruiting methyltransferase Prmt5. *Cell Rep.* **33**, 108490 (2020).
32. P. J. Metz *et al.*, Symmetric arginine dimethylation is selectively required for mRNA splicing and the initiation of type I and type III interferon signaling. *Cell Rep.* **30**, 1935–1950.e8 (2020).
33. F. Bachand, P. A. Silver, PRMT3 is a ribosomal protein methyltransferase that affects the cellular levels of ribosomal subunits. *EMBO J.* **23**, 2641–2650 (2004).
34. S. Miyata, Y. Mori, M. Tohyama, PRMT3 is essential for dendritic spine maturation in rat hippocampal neurons. *Brain Res.* **1352**, 11–20 (2010).
35. Y. Hu, Y. Su, Y. He, W. Liu, B. Xiao, Arginine methyltransferase PRMT3 promote tumorigenesis through regulating c-MYC stabilization in colorectal cancer. *Gene* **791**, 145718 (2021).
36. X. Zhang *et al.*, PRMT3 promotes tumorigenesis by methylating and stabilizing HIF1alpha in colorectal cancer. *Cell Death Dis.* **12**, 1066 (2021).
37. M. C. Hsu *et al.*, Protein arginine methyltransferase 3 enhances chemoresistance in pancreatic cancer by methylating hnRNPA1 to increase ABCG2 expression. *Cancers (Basel)* **11**, 8 (2018).
38. L. Unterholzner *et al.*, IFI16 is an innate immune sensor for intracellular DNA. *Nat. Immunol.* **11**, 997–1004 (2010).
39. H. Ishikawa, Z. Ma, G. N. Barber, STING regulates intracellular DNA-mediated, type I interferon-dependent innate immunity. *Nature* **461**, 788–792 (2009).
40. T. Abe *et al.*, STING recognition of cytoplasmic DNA instigates cellular defense. *Mol. Cell* **50**, 5–15 (2013).
41. H. Lian *et al.*, ZCCHC3 is a co-sensor of cGAS for dsDNA recognition in innate immune response. *Nat. Commun.* **9**, 3349 (2018).
42. R. Swiercz, D. Cheng, D. Kim, M. T. Bedford, Ribosomal protein rpS2 is hypomethylated in PRMT3-deficient mice. *J. Biol. Chem.* **282**, 16917–16923 (2007).
43. H. U. Kaniskan *et al.*, A potent, selective and cell-active allosteric inhibitor of protein arginine methyltransferase 3 (PRMT3). *Angew. Chem. Int. Ed. Engl.* **54**, 5166–5170 (2015).
44. S. Choi, C. R. Jung, J. Y. Kim, D. S. Im, PRMT3 inhibits ubiquitination of ribosomal protein S2 and together forms an active enzyme complex. *Biochim. Biophys. Acta* **1780**, 1062–1069 (2008).
45. R. S. Blanc, S. Richard, Arginine methylation: The coming of age. *Mol. Cell* **65**, 8–24 (2017).
46. X. Fan, T. Jin, Structures of RIG-I-like receptors and insights into viral RNA sensing. *Adv. Exp. Med. Biol.* **1172**, 157–188 (2019).
47. X. Zhang *et al.*, The cytosolic DNA sensor cGAS forms an oligomeric complex with DNA and undergoes switch-like conformational changes in the activation loop. *Cell Rep.* **6**, 421–430 (2014).
48. B. Liu, C. Gao, Regulation of MAVS activation through post-translational modifications. *Curr. Opin. Immunol.* **50**, 75–81 (2018).
49. J. Liu, C. Qian, X. Cao, Post-translational modification control of innate immunity. *Immunity* **45**, 15–30 (2016).
50. F. Rutsch *et al.*, A specific IFIH1 gain-of-function mutation causes Singleton-Merten syndrome. *Am. J. Hum. Genet.* **96**, 275–282 (2015).